

Low Energy Excitations in Spin Glasses from Exact Ground States

Matteo Palassini

University of California, 3333 California Street, Suite 415, San Francisco, CA 94118

Frauke Liers and Michael Jünger

Institut für Informatik, Universität zu Köln, D50969 Cologne, Germany

A. P. Young

Physics Department, University of California, Santa Cruz CA 95064

(Dated: May 21, 2019)

We investigate the nature of the low-energy, large-scale excitations in the three-dimensional Edwards-Anderson Ising spin glass with Gaussian couplings and free boundary conditions, by studying the response of the ground state to a coupling-dependent perturbation introduced previously. The ground states are determined *exactly* for system sizes up to 12^3 spins using a branch and cut algorithm. The data are consistent with a picture where the surface of the excitations is not space-filling, such as the droplet or the “TNT” picture. When allowing for large finite size corrections, the data are also consistent with a picture with space-filling surface, such as replica symmetry breaking. We compare the results with data for periodic boundary conditions obtained with a genetic algorithm, and discuss the effects of different boundary conditions on finite-size correction. Finally, we analyze the performance of our branch and cut algorithm, finding that it is correlated with the existence of large-scale, low-energy excitations.

PACS numbers: PACS numbers: 75.50.Lk, 75.40.Mg, 05.50.+q

I. INTRODUCTION

There is still considerable debate about the nature of the spin glass state in finite dimensional spin glasses. Two principal theories have been investigated: the “droplet theory” proposed by Fisher and Huse¹ (see also Refs. 2,3), and the replica symmetry breaking picture of Parisi^{4,5,6}. In the droplet theory the lowest energy excitation of length scale l (a “droplet”) has energy of order l^θ where θ is a positive exponent. Furthermore, the droplets have a surface with fractal dimension, d_s , less than the space dimension d .

Replica symmetry breaking (RSB) is well established in mean field theory, but it remains to be proven in finite dimensions. The precise nature of RSB in finite dimensions is not uniquely defined but it is generally agreed that a key feature of RSB is the existence of excitations whose energy, unlike that of droplets, remains of order unity even as their size tends to infinity. Furthermore, upon the creation of such a large scale, finite energy excitation, a finite fraction of the bonds change state (from satisfied to unsatisfied, or vice-versa) or, equivalently, the surface of these excitations is space filling, *i.e.* $d_s = d$.

Recently, Krzakala and Martin⁷ (KM), and two of us⁸ (PY), have argued, on the basis of numerical calculations at zero temperature, in favor of an intermediate scenario where there are large scale excitations whose energy does not increase with size, as in RSB, but which have a surface with $d_s < d$. Following KM we shall denote this the “TNT” scenario. In the TNT scenario it is necessary to introduce *two* exponents which describe the growth of the energy of an excitation of scale L : (i) θ (> 0) such that L^θ is the typical change in energy when the

boundary conditions are changed, for example from periodic to anti-periodic, in a system of size L , and (ii) θ' , which characterizes the energy of clusters excited within the system for a *fixed* set of boundary conditions (θ' was called θ_g in Ref.7). The TNT picture has been challenged (although in opposite senses) by Marinari and Parisi⁹ and by Middleton¹⁰. Subsequently, low temperature Monte Carlo simulations¹¹ have found results consistent with the TNT scenario. The RSB, droplet, TNT and some other scenarios have been also studied by Newman and Stein^{12,13}. For some recent related work, see Refs. 14,15.

The work of KM and PY determined the ground state with and without a certain perturbation (which was different in the two cases), designed so that the ground state of the perturbed system is a large scale excitation of the original system. They used *heuristic algorithms*, *i.e.* algorithms which are not *guaranteed* to give the exact ground state, although both KM and PY argue that they do find the exact ground state in most cases.

In this paper, we follow the perturbation approach of PY, described in Section II, but we apply an *exact* algorithm, known as “branch and cut”¹⁶, so we are guaranteed that the true ground state is reached every time. Exact optimization algorithms have been used before for spin glasses, see e.g. Refs. 17,18,19, but, to our knowledge, their use in three-dimensions has been restricted to smaller sizes than studied here, and they were not used to investigate the real-space structure of the low-energy excitations.

Our implementation of the branch and cut technique can handle significantly larger sizes for free boundary conditions (bc) than for periodic bc²⁰, so we use free bc here. We consider a different (and enlarged) set of ob-

servables than PY, and we also perform a similar analysis of the data of PY, who used periodic bc, in order to investigate the effects of different types of boundary conditions.

We find that for *periodic* bc, a simple scaling ansatz fits the results in a natural way, *i.e.* with negligible corrections to scaling and no adjustable parameters besides $d - d_s$ and θ' . This gives $d - d_s = 0.42 \pm 0.03$; $\theta' = -0.01 \pm 0.03$, which is in agreement with the results of PY, and is compatible with the TNT picture. We cannot rule out crossover to either the droplet or the RSB picture at length scales larger than our system sizes, but these scenarios would require larger corrections to scaling than the TNT picture.

For *free* bc, unlike for periodic bc, *all* forms of fitting require corrections to scaling. Making a natural assumption that the corrections to scaling are small we find $d - d_s = 0.45 \pm 0.02$; $\theta' = 0.18 \pm 0.03$, which is compatible with the droplet picture. However, if we allow for very large corrections to scaling, we also cannot rule out the TNT or RSB pictures.

We also analyze the performance of the branch and cut algorithm. The number of elementary operations required to find the ground state increases exponentially with the size, as expected since computing a ground state of a three-dimensional spin glass system is an \mathcal{NP} -hard problem²¹. We find that the CPU time is larger for samples in which there is an excited state close in energy to the ground state energy, yet different from the ground state in the orientation of a large number of spins. We are not aware of any previous quantitative measures of this trend, which we expect to be common to other algorithms as well.

The rest of this paper is organized as follows. In Section II we describe the method of perturbing the ground states to get information about low energy excitations introduced by PY. Our results for the nature of the large scale, low energy excitations are given in Section III. A short description of the branch and cut algorithm used is given in Section IV, and the performance of the algorithm is analyzed in Section V. Our conclusions are summarized in Section VI.

II. GROUND STATE PERTURBATION METHOD

The Hamiltonian of the spin glass model is given by

$$\mathcal{H} = - \sum_{\langle i,j \rangle} J_{ij} S_i S_j, \quad (1)$$

where the sites i lie on a simple cubic lattice with $N = L^3$ spins in dimension $d = 3$, $S_i = \pm 1$, and the J_{ij} are nearest-neighbor interactions chosen from a Gaussian distribution with zero mean and standard deviation unity. Free boundary conditions are applied in all directions.

For a given set of bonds we determine the exact ground state using a branch and cut algorithm discussed in Sec-

tion IV. Let $S_i^{(0)}$ be the ground state spin configuration. As in PY we then perturb the couplings J_{ij} by an amount proportional to $S_i^{(0)} S_j^{(0)}$ in order to increase the energy of the ground state relative to the other states and therefore possibly induce a change in the ground state. This perturbation, which depends upon a positive parameter ϵ , is defined by

$$\Delta \mathcal{H}(\epsilon) = \epsilon \frac{1}{N_b} \sum_{\langle i,j \rangle} S_i^{(0)} S_j^{(0)} S_i S_j, \quad (2)$$

where $N_b = dL^{d-1}(L-1)$ is the number of bonds in the Hamiltonian. We denote the unperturbed ground state energy by $E^{(0)}$ and the perturbed energy of the *same* state by $\tilde{E}^{(0)}$. The energy of the unperturbed ground state will thus increase exactly by an amount $\Delta E^{(0)} \equiv \tilde{E}^{(0)} - E^{(0)} = \epsilon$. The energy of any other state, α say, will increase by the lesser amount $\Delta E^{(\alpha)} \equiv \tilde{E}^{(\alpha)} - E^{(\alpha)} = \epsilon q_l^{(0,\alpha)}$, where $q_l^{(0,\alpha)}$ is the “link overlap” between the states “0” and α , defined by

$$q_l^{(0,\alpha)} = \frac{1}{N_b} \sum_{\langle i,j \rangle} S_i^{(0)} S_j^{(0)} S_i^{(\alpha)} S_j^{(\alpha)}, \quad (3)$$

in which the sum is over all the N_b nearest neighbor bonds. Note that the *total* energy of the states changes by an amount of order unity.

As we apply the perturbation, the energy *difference* between a low energy excited state and the ground state decreases by the amount

$$\Delta E^{(0)} - \Delta E^{(\alpha)} = \epsilon (1 - q_l^{(0,\alpha)}). \quad (4)$$

If there is at least one excited state such that $E^{(\alpha)} - E^{(0)} < \Delta E^{(0)} - \Delta E^{(\alpha)}$, then one of these excited states will become the ground state of the perturbed Hamiltonian. We denote the new ground state spin configuration by $\tilde{S}_i^{(0)}$, and indicate by q_l and q , with no indices, the link- and spin-overlap between the new and old ground states $S_i^{(0)}$ and $\tilde{S}_i^{(0)}$, where q is defined as usual by $q = 1/N \sum S_i^{(0)} \tilde{S}_i^{(0)}$.

Due to the spin flip symmetry of the Hamiltonian (1), the ground state is doubly degenerate, and therefore the distribution of q is symmetric²² around $q = 0$. Hence, in the rest of the paper we will restrict ourselves to $q \geq 0$ without loss of information.

Consider the probability $P(\epsilon, L)$ (with respect to the random couplings) that q is less than unity, *i.e.* that $S_i^{(0)}$ and $\tilde{S}_i^{(0)}$ differ in a finite fraction of the spins. As discussed by PY, we assume that $P(\epsilon, L)$ is dominated by those samples in which $S_i^{(0)}$ and $\tilde{S}_i^{(0)}$ differ by flipping a single connected cluster of spins, with linear size L . Deviations from this assumption give rise to corrections to scaling, as pointed out by Middleton¹⁰, and will be analyzed in Section III. There are two energy scales in the problem: the typical energy above the ground state of such an excitation, which scales as $L^{\theta'}$ ($\theta' = \theta$ in the

droplet picture), and the threshold energy of Eq. (4), which scales as $\epsilon L^{-(d-d_s)}$ since $1 - q_l$ is proportional to the surface of the excitation, $1 - q_l \sim L^{-(d-d_s)}$. Hence, the dimensionless probability $P(\epsilon, L)$ is a function of the ratio of these two energy scales:

$$P(\epsilon, L) = g(\epsilon L^{-\mu}), \quad (5)$$

where $g(x)$ is a scaling function and

$$\mu \equiv \theta' + d - d_s. \quad (6)$$

From this we obtain scaling relations for various observables. For example, since $1 - q \sim O(1)$ and $1 - q_l \sim L^{-(d-d_s)}$, we obtain⁸:

$$\langle 1 - q \rangle = F_q(\epsilon L^{-\mu}) \quad (7)$$

$$\langle 1 - q_l \rangle = L^{-(d-d_s)} F_{q_l}(\epsilon L^{-\mu}), \quad (8)$$

where $\langle \dots \rangle$ is the average with respect to the random couplings. By measuring $\langle 1 - q \rangle$ and $\langle 1 - q_l \rangle$ we can then determine $d - d_s$ and θ' , and discriminate between the various pictures discussed in Section I.

For small ϵ , we expect the probability that the ground state changes to be proportional to ϵ (for fixed L), which implies $g(x) \sim x$ for $x \rightarrow 0$. Hence $F_q(x)$ and $F_{q_l}(x)$ also vary linearly for small x , and the *asymptotic* behavior for $L \gg \epsilon^{1/\mu}$ is

$$\langle 1 - q \rangle \sim \epsilon L^{-\mu}, \quad (9)$$

$$\langle 1 - q_l \rangle \sim \epsilon L^{-\mu}, \quad (10)$$

where

$$\mu_l \equiv \theta' + 2(d - d_s). \quad (11)$$

In the RSB case, $d - d_s = \theta' = 0$, and therefore $\mu = \mu_l = 0$. The scaling relations in Eqs. (7, 8) reduce in this case to

$$\langle 1 - q \rangle = F_q(\epsilon), \quad \langle 1 - q_l \rangle = F_{q_l}(\epsilon) \quad (\text{RSB}), \quad (12)$$

and the asymptotic behavior for $L \rightarrow \infty$ to

$$\langle 1 - q \rangle, \quad \langle 1 - q_l \rangle \sim \epsilon \quad (\text{RSB}) \quad (13)$$

It is also convenient to analyze just those samples in which the unperturbed and perturbed ground states are very different, i.e. where $q \leq q_{\max}$, a threshold value. Denoting such restricted averages by $\langle \dots \rangle_c$, we have

$$\langle 1 - q_l \rangle_c = L^{-(d-d_s)} F_{q_l}^c(\epsilon L^{-\mu}). \quad (14)$$

This is of the same form as in Eq. (8), but, for sufficiently small q_{\max} , the behavior of the scaling functions $F_{q_l}(x)$ and $F_{q_l}^c(x)$ at small argument will be different for the following reason. If we average over all samples we need to include the probability $P(\epsilon, L)$ that the perturbation generates an excitation with $q < 1$. This is proportional to $\epsilon L^{-\mu}$ for $\epsilon L^{-\mu} \ll 1$, which is the reason why

$F_q(x) \sim x$ for small x . However, this factor is automatically taken into account in the *selection* of the samples in the restricted average in Eq. (14), and so should not be included again when performing the average. As a result, $F_{q_l}^c(x)$ tends to a constant for $x \rightarrow 0$ and the asymptotic behavior at large L is

$$\langle 1 - q_l \rangle_c \sim L^{-(d-d_s)}. \quad (15)$$

In particular, in RSB this becomes

$$\langle 1 - q_l \rangle_c \sim \text{const.} \quad (\text{RSB}). \quad (16)$$

Note that in both cases the asymptotic behavior is *independent* of ϵ .

When analyzing the numerical data, we must be aware that there are corrections to finite-size scaling which occur when L is not large enough. These take the form of *additive* corrections to scaling relations such as Eqs. (5), (7), (8), and (14), whose amplitude is characterized by a correction to scaling exponent ω . For example, including the leading correction, Eq. (14) becomes

$$\langle 1 - q_l \rangle_c = \frac{1}{L^{d-d_s}} \left\{ F_{q_l}^c(\epsilon L^{-\mu}) + \frac{1}{L^\omega} G_{q_l}(\epsilon L^{-\mu}) \right\}, \quad (17)$$

and for $\epsilon L^{-\mu} \rightarrow 0$, the asymptotic result corresponding to Eq. (15) is

$$\langle 1 - q_l \rangle_c = \frac{1}{L^{d-d_s}} \left(a + \frac{b}{L^\omega} \right). \quad (18)$$

For the RSB case, this goes over to

$$\langle 1 - q_l \rangle_c = a + \frac{b}{L^\omega}, \quad (19)$$

rather than Eq. (16).

Even when these corrections are negligible and the scaling *form*, such as Eq. (14), is valid, the argument of the scaling function may not be sufficiently small for a simple power law dependency of the data on system size, such as Eq. (15), to be valid. In this regime, expanding the scaling function gives rise to *further* additive corrections to the *asymptotic* behavior. For example, the leading correction to Eq. (15), coming from expanding the $F_{q_l}^c$ in Eq. (14) to second order, will be

$$\langle 1 - q_l \rangle_c = \frac{1}{L^{d-d_s}} \left(a + b \frac{\epsilon}{L^\mu} \right) \quad (20)$$

which goes over to $\langle 1 - q_l \rangle_c = a + b \epsilon$ in RSB. In general, both types of corrections need to be borne in mind when fitting the data.

III. RESULTS

We applied the perturbation method described in the previous Section to systems of size $L = 4, 6, 8, 10$, and

L	$\epsilon/\tau = \frac{1}{4}$	$\epsilon/\tau = \frac{1}{2}$	$\epsilon/\tau = 1$	$\epsilon/\tau = 2$	$\epsilon/\tau = 4$
4	50000	50000	50000	50000	50000
6	20000	20000	20000	20000	20000
8	15000	13467	13467	6000	6000
10	10000	7440	6000	4918	4000
12	5670		4202		

TABLE I: Number of independent realizations of the disorder (samples) used in the computations.

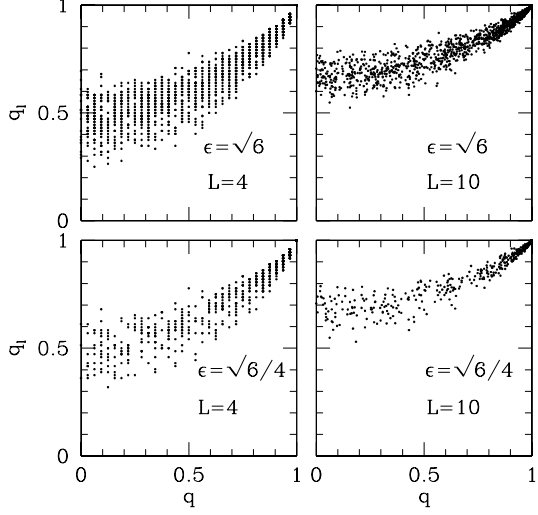


FIG. 1: Scatter plots in the (q, q_l) plane.

12. For each size, we considered five values of the perturbation strength ϵ , namely $\epsilon/\tau = \frac{1}{4}, \frac{1}{2}, 1, 2$, and 4, where $\tau = \sqrt{6}$ is the mean field transition temperature, except for $L = 12$ for which only $\epsilon/\tau = \frac{1}{4}$ and 1 were considered. We choose this value of τ so we can compare our results with the results of PY for periodic bc. In order to discriminate between the different pictures, it is important to have high statistics. Table I reports the number of samples computed for each size. Note that the number of samples necessary to achieve a given statistical error increases as ϵ decreases, since the fraction of samples in which the $\tilde{S}^{(0)} \neq S^{(0)}$ also decreases.

A. Spin and link overlap

1. Qualitative analysis

We start with a qualitative analysis of the results. In Fig. 1, we show scatter plots in the (q, q_l) plane for $L =$

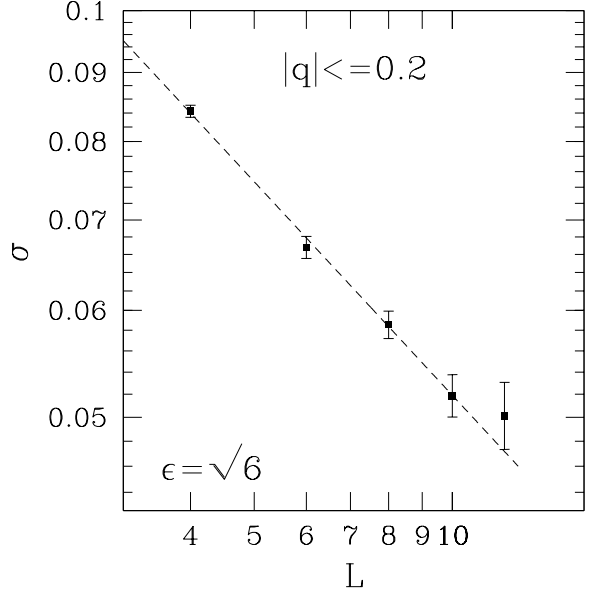


FIG. 2: A plot of the standard deviation of the link-overlap $\sigma = (\langle q_l^2 \rangle_c - \langle q_l \rangle_c^2)^{1/2}$, where the average is restricted to samples such that $q_l \leq 0.2$. The line represents a power law fit with exponent $\delta = 0.52$.

4, 10 and $\epsilon/\tau = \frac{1}{4}, 1$, where each point represents one of 2000 randomly generated samples. Clearly, the link- and spin-overlap are strongly correlated. We note that, as ϵ decreases, there are less points with $q_l < 1$, and that as L increases the data shift towards $q_l = 1$. Similar plots²³ for periodic bc show that q_l is significantly lower than for free bc. While q has a large variance (the points are distributed along the whole q axis), the link-overlap has a much smaller variance, which decreases as L increases, suggesting that in the thermodynamic limit q_l becomes a well defined function of q .

In Fig. 2 we show the standard deviation of q_l for the restricted average over those samples where $q_l \leq q_{max}$, i.e.

$$\sigma = \sqrt{\langle q_l^2 \rangle_c - \langle q_l \rangle_c^2}, \quad (21)$$

as a function of the system size for $\epsilon/\tau = 1$. Here and in the following, $\langle \dots \rangle_c$ denotes a conditional sample average restricted to an interval of values for q . Here we take $q_{max} = 0.2$, since we are interested in the region of small q , which corresponds to large-scale excitations. A power law fit $\sigma = aL^{-\delta}$ gives $\delta = 0.52 \pm 0.03$ ($\chi^2 = 1.80$, the best fit is shown in Fig. 2). We have also considered the effect of restricting the average in Eq. (21) to different intervals $q \in [q_{min}, q_{max}]$. For the whole range of q values, the data for σ are again compatible with a power law. A vanishing σ in the thermodynamic limit is consistent with RSB, which predicts that q_l is a (nontrivial) function of q . A vanishing σ is also trivially consistent with the droplet

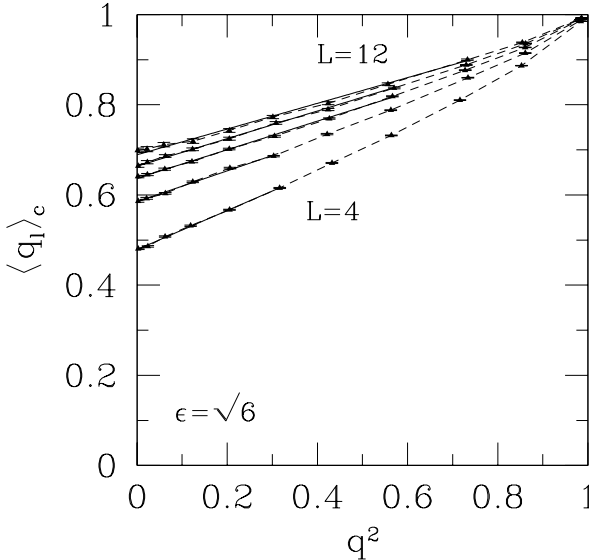


FIG. 3: Average of the link-overlap restricted to intervals of q of width 0.1, as a function of q for different sizes L (from bottom to top, $L = 4, 6, 8, 10, 12$). The continuous lines represent quadratic fits including values of q up to where the lines end. The dashed lines are a guide to the eye.

model or the TNT picture, where $q_l = 1$ for all q .

Under the RSB hypothesis, it is interesting to study the functional relationship between q and q_l . In Fig. 3 we show the *average* value of q_l , restricted to intervals $q \in [q_{\min}, q_{\max}]$, as a function of the mean value of q in each interval²⁴ for $\epsilon/\tau = 1$. A quadratic form $q_l = \alpha(L) + \beta(L) q^2$, motivated by the infinite-range Sherrington-Kirkpatrick model where $q_l = q^2$, fits well the data for q less than some cut-off value which increases with L (see Fig. 3). The quadratic fit works well also for other values of ϵ , and $\alpha(L)$ and $\beta(L)$ show a modest variation with ϵ . We also tried global fits including data for all values of q and L , obtaining similar results.

Extrapolating $\alpha(L)$ and $\beta(L)$ to $L \rightarrow \infty$ with fits of the form $\alpha(L) = \alpha + c/L^d$, $\beta(L) = \beta + c/L^d$, we obtain

$$q_l = (0.77 \pm 0.02) + (0.27 \pm 0.03) q^2. \quad (22)$$

This nontrivial relation between q and q_l in the thermodynamic limit is consistent with RSB, while in the droplet or TNT pictures the data in Fig.3 would shift to $q_l \equiv 1$ in this limit. In the following, we will investigate in more detail the validity of the various pictures.

2. Determination of $d - d_s$

Fig. 4 plots $\langle 1 - q_l \rangle_c$ as a function of L , for various values of ϵ and $q_{\max} = 0.4$ ($q_{\max} = 0.2$ gives essentially the same results).

First, note that, independently of what picture holds in the $L \rightarrow \infty$ limit, the data of Fig. 4 deviate significantly from the asymptotic behavior, see Eq. (15), in which the various ϵ values should collapse on a single curve.

Second, the data have a noticeable positive (upward) curvature for all values of ϵ . In Section III C we will show that in the case of periodic bc the data have a much smaller dependence on ϵ and a much smaller curvature (see Fig. 11).

We fitted the data of Fig. 4 (by χ^2 minimization) with the following three functional forms:

$$\begin{aligned} \text{Form I: } & \langle 1 - q_l \rangle_c = a + b/L^c \\ \text{Form II: } & \langle 1 - q_l \rangle_c = a + b/L + c/L^2 \\ \text{Form III: } & \langle 1 - q_l \rangle_c = b/L^c \end{aligned} \quad (23)$$

Form I corresponds to the RSB prediction including the leading correction to scaling, see Eq. (19), with $c \equiv \omega$. Form II is a different parameterization of the correction to scaling for RSB, considered by Marinari and Parisi⁹. Form III corresponds to the asymptotic behavior of both the TNT and droplet pictures *without* corrections to scaling, see Eq. (15), with $c \equiv d - d_s$.

The results of these fits are reported in Table II. Forms I and II, appropriate to RSB, fit well the data with a low χ^2 and $a > 0$ outside the error bars. The best fits with Form I are shown by the dashed lines in Fig. 4. The variation of a between Forms I and II provides a measure of the systematic error associated with the unknown corrections to scaling. Within this error, a is independent of ϵ , as predicted by RSB. Therefore, the data for $\langle 1 - q_l \rangle_c$ are compatible with RSB, and our central estimate under the RSB hypothesis is

$$\lim_{L \rightarrow \infty} \langle 1 - q_l \rangle_c = 0.20 \pm 0.02 \quad (\text{RSB}). \quad (24)$$

Marinari and Parisi⁹ fitted Form I (resp. II) to their data for periodic boundary conditions, $L \leq 14$, and $\epsilon/\tau = 4$, and obtained $a = 0.24$ (resp. $a = 0.30$), from which we estimate a central value $a = 0.27 \pm 0.05$. This is just in agreement with our estimate above for free bc, suggesting that the infinite volume limit of $\langle 1 - q_l \rangle_c$ may be independent of the boundary conditions, although we do not have an argument why this should be the case.

The power law Form, III, appropriate to the droplet model or the TNT scenario, fits well the data for $\epsilon/\tau < 2$ if we exclude $L = 4$, and the fit parameters b and c are almost independent of ϵ . The quality of the fit of Form III is worse than that of Forms I and II, as also noted in Ref.9. However, we stress that this fact alone does *not* necessarily favor the RSB picture, since Form III does not include corrections to scaling, while Forms I and II do.

A better comparison requires then to include corrections to scaling to Form III. To this end, we tried fits with

$$\text{Form IV: } L^{d-d_s} \langle 1 - q_l \rangle_c = a + b/L^c \quad (25)$$

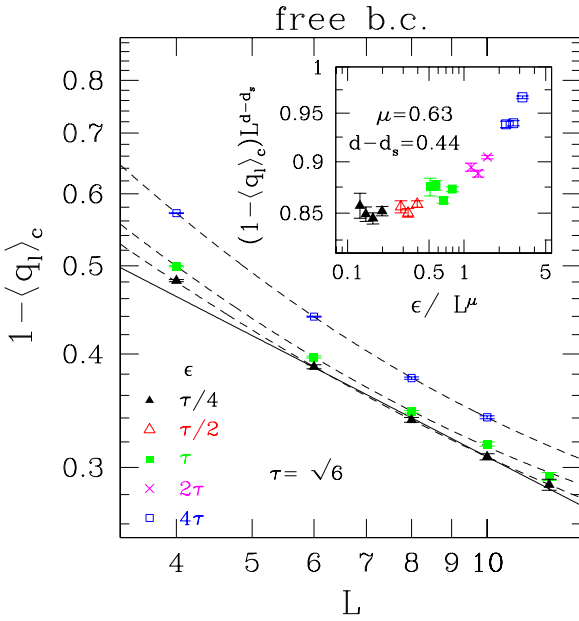


FIG. 4: Logarithmic plot of the average $\langle 1 - q_l \rangle_c$, restricted to samples with $|q| \leq 0.4$, as a function of the system size L . Only three values of ϵ are displayed for clarity. The lower continuous line is the best fit with a power-law, Form III in Eq. (23) for $\epsilon/\tau = \frac{1}{4}$, where $\tau = \sqrt{6}$, and the $L = 4$ data have been excluded from the fit. The dashed lines are the best fits with Form I in Eq. (23). The inset shows a scaling plot of the data in the main figure, excluding the $L = 4$ data, according to Eq. (14). Here and in the following figures, note that the data for various ϵ are correlated, since the samples used for large ϵ were also used for small ϵ .

where we fix $d - d_s$. This fits well the data for a wide range of values of $d - d_s$. For example, for $\epsilon/\tau = \frac{1}{4}$, a value of $d - d_s$ between 0 and 0.45 gives a goodness-of-fit parameter $Q \geq 0.43$, which is acceptable.

This shows that, when properly including corrections to scaling, the droplet or TNT pictures fit the data with a goodness of fit comparable to RSB. However, two comments are in order. First, within the interval of acceptable values of $d - d_s$, the larger is $d - d_s$ the smaller are the corrections to the asymptotic behavior. Hence a value of $d - d_s$ around 0.44 may be regarded as more ‘‘natural’’ in this range of sizes, since it gives the smallest corrections. For example, for $\epsilon/\tau = \frac{1}{4}$ and $d - d_s = 0.42$, the correction term b/L^c in Form IV amounts to only 0.1% of the total for $L = 12$, while for $d - d_s = 0$ it amounts to 43%. By imposing that the correction to scaling for $L \geq 8$ is less than 3%, we obtain the estimate

$$d - d_s = 0.44 \pm 0.03 \quad (26)$$

where the error is purely statistical. In Table II we show the fits obtained with Form IV imposing this value. This is in agreement with the estimate $d - d_s = 0.42 \pm 0.02$ of PY for periodic bc (see also Section III C of this paper),

Form	ϵ/τ	χ^2	Q	a	b	c
I	0.25	0.014	0.99	0.171(2)	1.068(5)	0.890(8)
	0.5	0.015	0.90	0.185(2)	1.14(1)	0.96(1)
	1	3.04	0.22	0.201(14)	1.26(7)	1.04(7)
	2	0.39	0.52	0.206(6)	1.42(3)	1.08(3)
II	0.25	0.037	0.98	0.182(1)	1.29(2)	-0.40(5)
	0.5	0.010	0.92	0.189(1)	1.23(1)	-0.14(3)
	1	3.01	0.22	0.198(8)	1.16(10)	0.16(27)
	2	0.47	0.49	0.199(4)	1.21(5)	0.31(14)
III	0.25	1.40	0.49		0.85(2)	0.44(1)
	0.5	1.63	0.20		0.87(3)	0.45(2)
	1	9.81	0.007		0.88(3)	0.44(2)
	2	6.75	0.009		0.95(4)	0.47(2)
IV	0.25	0.0007			1.09(5)	0.51(2)
	0.5	0.55	0.76	0.808(4)	7(8)	3.6(8)
	1	5.91	0.05	0.828(7)	18(37)	4.0(1.5)
	2	2.80	0.09	0.844(9)	5(5)	2.9(7)
	4	3.01	0.08	0.87(1)	3.8(1.6)	2.3(3)

TABLE II: Fits to $\langle 1 - q_l \rangle_c$ with $q_{\min} = 0$ and $q_{\max} = 0.4$. The four groups of data refer, from top to bottom, to the three fitting functions I, II, and III in Eq. (23), and Form IV in Eq. (25) with $d - d_s = 0.44$. For Form III, data for $L = 4$ was not included in the fit. The errors are the standard errors of a nonlinear fitting routine²⁵, and Q is the goodness-of-fit parameter.

which is reassuring since $d - d_s$ should not depend on the boundary conditions. We note that if Forms I or II, appropriate to RSB, describe the true asymptotic behavior, corrections within 3% from the asymptotic limit would only be attained for a size $L \simeq 200$.

Second, as we discussed in Section II, even in the regime where corrections to scaling are negligible, the asymptotic power-law behavior (under the hypothesis $d - d_s > 0$) sets in only for $L \gg \epsilon^{1/\mu}$. This would explain why, if $d - d_s \simeq 0.44$, the quality of the power-law fit becomes progressively worse as ϵ increases.

The deviation from the asymptotic behavior appears to be very significant for $\epsilon/\tau = 4$, and hence from the data of $\epsilon/\tau = 4$ alone we should not necessarily conclude⁹ that an asymptotic power-law behavior is ruled out. This is seen also in the inset of Fig. 4, which shows that, if we exclude $L = 4$, the data are compatible with the scaling relation Eq. (8), where the exponent μ is independently determined below.

PY determined $d - d_s$ from the ratio $R = \langle 1 - q_l \rangle / \langle 1 - q \rangle$ which has the same scaling behavior as the quantity $\langle 1 - q_l \rangle_c$ used here, namely $R = L^{-(d - d_s)} F_R(\epsilon/L^\mu)$, with $F_R(x) \sim \text{const.}$ as $x \rightarrow 0$. Middleton¹⁰ observed that, in two dimensions, small droplets introduce significant cor-

rections to scaling, and suggested that this may be the case also in three dimensions, possibly invalidating the conclusions of PY. The quantity $\langle 1 - q_l \rangle_c$ is less sensitive to these corrections since, by restricting to small q , small droplets give a smaller contribution. Hence, to investigate these corrections, we fitted our data for R with the three functional forms of Eq. (23) (with R replacing $\langle 1 - q_l \rangle_c$). Forms I and II fit well the data with a low χ^2 , giving $a = 0.27 \pm 0.03$ independent of ϵ within the error bars. A power law fits well the data if we exclude $L = 4$, with an exponent $d - d_s = 0.43 \pm 0.03$ nearly independent of ϵ and in agreement with Eq. (26). The residual dependence on ϵ is well accounted for by a scaling plot similar to the inset in Fig. 4. As for $\langle 1 - q_l \rangle_c$, Form IV also fits well the data for a wide range of values of $d - d_s$. Again, a power law is more natural in the sense that corrections to scaling are smaller. We interpret the fact that $\langle 1 - q_l \rangle_c$ and R give the same value of $d - d_s$ in a power law fit, as evidence that corrections due to small droplets are indeed not important in three dimensions in this range of sizes. In Section III C we will show that this is also the case for periodic bc.

To summarize this part, the data are compatible with a wide range of values of $d - d_s$ between 0 and 0.45, but a value at the higher end of this range describes the data in a more natural way, in the sense that the corrections to scaling are smaller.

3. Determination of μ

Next, we turn to the exponent μ defined in Eq. (6). To this end we consider the ratio

$$B = \frac{\langle 1 - q_l \rangle^2}{\langle (1 - q_l)^2 \rangle} \quad (27)$$

which scales as

$$B = F_B(\epsilon/L^\mu). \quad (28)$$

The factor L^{d-d_s} does not appear here since it cancels between numerator and denominator of Eq. (27), thus allowing us to determine μ independently of $d - d_s$. Following the arguments in Section II, we expect $F_B(x) \sim x$ for small x since both $L^{d-d_s} \langle 1 - q_l \rangle$ and $L^{2(d-d_s)} \langle (1 - q_l)^2 \rangle$ vary as ϵ/L^μ for $\epsilon/L^\mu \rightarrow 0$.

We fit Eq. (28) to our data assuming a polynomial form of order n for $F_B(x)$, with the coefficient of x^0 set to zero so that $F_B(x) \sim x$ as $x \rightarrow 0$, and we determine the value of μ which gives the best fit, varying n until the χ^2 of the best fit becomes approximately constant. In this way we obtain

$$\mu = 0.63 \pm 0.03 \quad (29)$$

As shown in Fig. 5, scaling is quite satisfactory, although the data for different ϵ overlap only slightly. The best fit for $n = 6$ is displayed by the continuous line. We

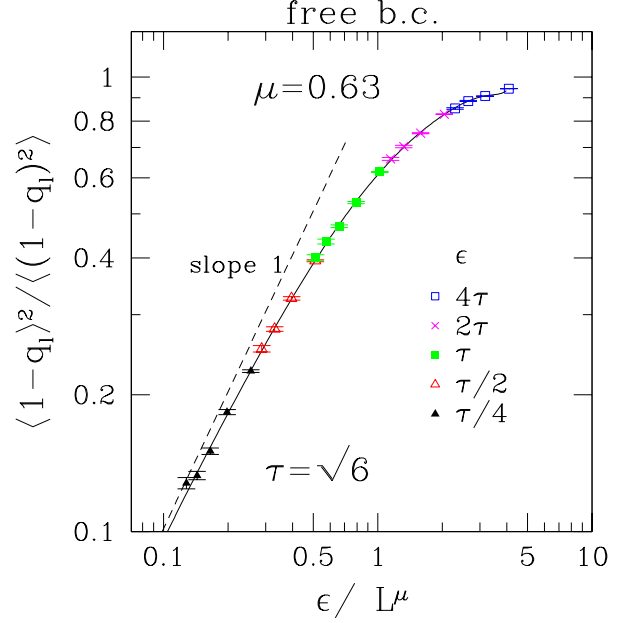


FIG. 5: Scaling plot of the ratio $B = \langle 1 - q_l \rangle^2 / \langle (1 - q_l)^2 \rangle$ according to Eq. (28). The continuous line is a polynomial fit of order $n = 6$, which gives $\chi^2/\text{d.o.f} = 1.09$, and a goodness-of-fit parameter $Q = 0.35$. The dashed line is the linear term of the polynomial fit, corresponding to the asymptotic behavior for $L \rightarrow \infty$.

emphasize that this scaling plot is obtained with only one adjustable parameter, μ . The dashed line in Fig. 5 represents the linear term of $F_B(x)$, and the deviation from this line gives a measure of the corrections to the power-law asymptotic behavior. The $\epsilon/\tau = \frac{1}{4}$ data are quite close to the asymptotic behavior, while the data for large ϵ deviate significantly from it, since B must satisfy the inequality $B \leq 1$.

In RSB, $B \sim \epsilon$ as $L \rightarrow \infty$. To test this prediction, we performed fits of B using the fitting functions Form I and Form II in Eq. (23), (where $\langle 1 - q_l \rangle_c$ is replaced by B). Form I gives unphysical (negative) values of a , while Form II gives an acceptable fit with a positive a roughly proportional to ϵ . Therefore, the data for B cannot rule out RSB. Note however that, if RSB hold, the scaling in Fig. 5 would be accidental, and would not hold for larger sizes.

We can obtain a second estimate of μ from the quantity $\langle 1 - q_l \rangle$ (q unrestricted), which scales as in Eq. (8), and has the asymptotic behavior of Eq. (10) for $\epsilon/L^\mu \rightarrow 0$. By fitting the data using the three functional forms of Eq. (23) (where now $\langle 1 - q_l \rangle_c$ is replaced by $\langle 1 - q_l \rangle$), we find that Form I fits well the data, with a roughly proportional to ϵ as expected in RSB, although, for small ϵ , a is also compatible with zero. A power law fit $\langle 1 - q_l \rangle = b/L^\mu$ (Form III) gives acceptable fits for $\epsilon/\tau \leq \frac{1}{2}$ and for all values of ϵ if we exclude $L = 4$. The exponent μ_l changes significantly with ϵ , presumably due to corrections to

scaling, and by extrapolating it to $\epsilon = 0$ we obtain $\mu_l = 1.15 \pm 0.08$. This gives $\mu = \mu_l - (d - d_s) = 0.60 \pm 0.09$ which agrees with the estimate $\mu = 0.63 \pm 0.03$ obtained from B . We also verified that the scaling relation Eq. (8) describes reasonably well the data for $\mu = 0.64 \pm 0.05$.

In the above analysis, we have determined the exponents μ and $d - d_s$ using just the link-overlap q_l . By contrast, PY determined μ (for periodic bc) from the scaling of the spin-overlap q . An advantage of q_l is that its variance is much lower, as shown in Fig. 1. In any event, we have verified that the scaling relation Eq. (7) fits well the data for q , giving $\mu = 0.65 \pm 0.02$, in agreement with the estimate from B .

Summarizing this part, we find that the data are consistent with the RSB prediction that $\mu = 0$ asymptotically, but large corrections to scaling are required in the fit. However, by imposing that the corrections to scaling are small, we obtain the value $\mu \simeq 0.63$. Under this assumption, from the estimates of μ and $d - d_s$ in Eqs. (29) and (26), we obtain

$$\theta' = \mu - (d - d_s) = 0.19 \pm 0.06. \quad (30)$$

This result agrees with the droplet theory which predicts that $\theta' = \theta > 0$, and is compatible with the value of $\theta \simeq 0.2$ characterizing the energy of domain walls induced by a change in boundary conditions²⁶. By contrast, for periodic bc θ' is compatible with zero (see PY and Section III C). In Section III C we will analyze the origin of this discrepancy.

B. Box overlaps

So far we have analyzed the link-overlap. We now turn to a different observable, the *box-overlap* defined as

$$q_B = \frac{1}{L_B^d} \sum_i S_i^{(0)} \tilde{S}_i^{(0)} \quad (31)$$

where the sum runs over the sites contained in a central cubic box of *fixed* size $L_B = 2$. In the following we will only consider the absolute value $|q_B|$, which we still call q_B for simplicity. When a large-scale cluster of spins is flipped, for large L the probability that its surface goes across the central box is proportional to the ratio of its surface area, $\sim L^{d_s}$, to the volume, L^d . Therefore $1 - q_B \sim L^{-(d - d_s)}$ from which we obtain the scaling laws

$$\langle 1 - q_B \rangle = L^{-(d - d_s)} F_{q_B}(\epsilon/L^\mu) \quad (32)$$

$$\langle 1 - q_B \rangle_c = L^{-(d - d_s)} F_{q_B}^c(\epsilon/L^\mu) \quad (33)$$

where, as for the corresponding scaling functions for q_l , $F_{q_B}(x) \sim x$ and $F_{q_B}^c(x) \sim \text{const.}$ for small x . Hence the asymptotic scaling for $L \rightarrow \infty$ is

$$\langle 1 - q_B \rangle \sim \epsilon L^{-\mu} \quad (34)$$

$$\langle 1 - q_B \rangle_c \sim L^{-(d - d_s)}. \quad (35)$$

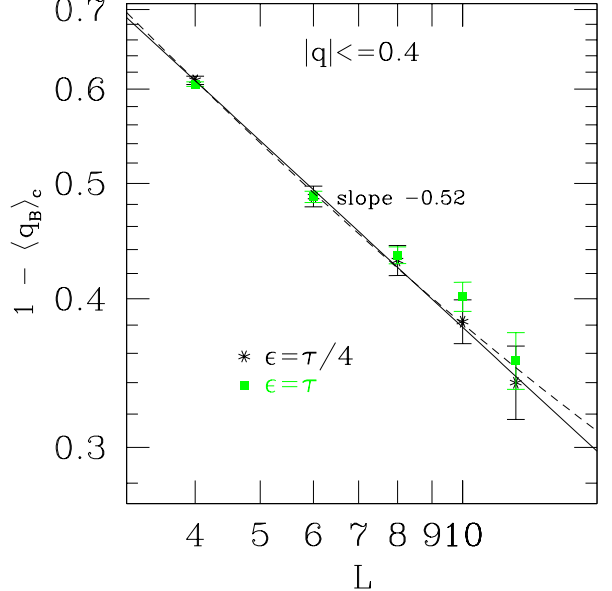


FIG. 6: Logarithmic plot of the average box-overlap, restricted to samples such that $q \leq 0.4$. We show the data for just two values of ϵ for clarity. The data for other values of ϵ are superimposed. The lower continuous line is a power-law fit for $\epsilon/\tau = 4$. The dashed line is the fit with Form II in Eq. (23), with q_B replacing q_l . The slope gives the exponent $d - d_s$.

In RSB, this reduces to $\langle 1 - q_B \rangle \sim \epsilon$ and $\langle 1 - q_B \rangle_c \sim \text{const.}$ An advantage of q_B over q_l is that the former, being measured away from the boundaries, should have smaller corrections to scaling and be less sensitive to boundary conditions. Indeed, Monte Carlo simulations^{27,28} show that q_B has rather small corrections to scaling. This is likely to be particularly important for the free boundary conditions used here.

Fig. 6 shows the *restricted* average $\langle 1 - q_B \rangle_c$, with $q_{\max} = 0.4$, as a function of L for two values of ϵ . The data are clearly decreasing with L , are essentially independent of ϵ , as expected from Eq. (35), and are close to a straight line on the logarithmic plot. This indicates that the power law fit, Form III, appropriate to the droplet and TNT scenarios, should work well and indeed it does, even for the largest value of ϵ (we note however that the statistical errors are larger than for the link-overlap). The exponent is almost independent of ϵ , varying between 0.48 and 0.52, and from this we obtain the estimate

$$d - d_s = 0.48 \pm 0.03 \quad (36)$$

which is in agreement with the estimates $d - d_s = 0.44 \pm 0.03$ from $\langle 1 - q_l \rangle_c$ and $d - d_s = 0.43 \pm 0.03$ from R .

Forms I and II in Eq. (23) (with q_B replacing q_l) also fit well the data, with a between 0.14 and 0.36 (with no discernible trend with ϵ). Hence the data are also

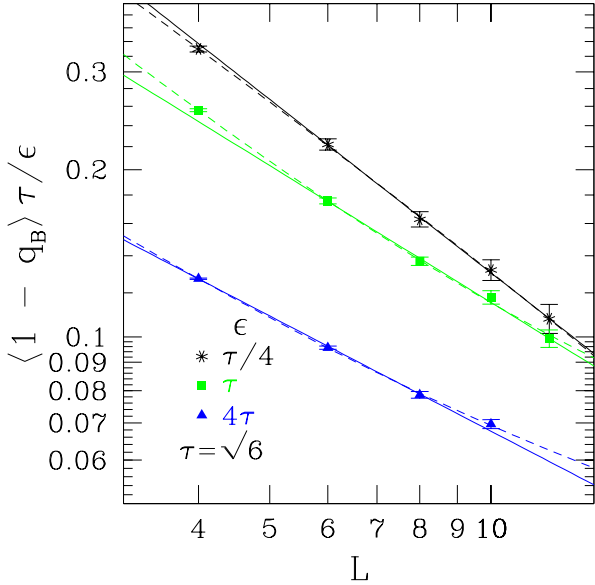


FIG. 7: Logarithmic plot of the average box-overlap, multiplied by τ/ϵ in order to highlight the deviation from the asymptotic behavior of Eq. (34) in which the data for various ϵ should collapse on a single curve. The continuous lines represent fits with the power-law Form III excluding $L = 4$. The dashed lines represent fits with Form I in Eq. (23).

compatible with RSB, and under the RSB hypothesis, we estimate

$$\lim_{L \rightarrow \infty} \langle 1 - q_B \rangle_c = 0.25 \pm 0.10 \quad (\text{RSB}). \quad (37)$$

Fig. 7 shows the unrestricted average $\langle 1 - q_B \rangle$ multiplied by τ/ϵ , which asymptotically should be independent of ϵ . The data show a small curvature and a significant ϵ dependence, indicating that for this quantity we are not yet in the asymptotic region (similarly to what we observed for the quantity B). The data are fitted well by a power law, and fits using Forms I and II give a compatible with zero. We determined μ from the scaling relation Eq. (32), by fixing $d - d_s = 0.44$ and using the same fitting procedure as for B , finding

$$\mu = 0.62 \pm 0.04 \quad (38)$$

which agrees with the various estimates of μ obtained from B , $\langle 1 - q_l \rangle$, and $\langle 1 - q \rangle$. Fig. 8 shows the corresponding scaling plot.

To conclude this subsection, the data for box overlaps can be fitted with smaller corrections to scaling than the data for the (bulk) link overlap. Assuming a power law fit, appropriate for the droplet or TNT scenarios, with no corrections to scaling, the final results for the exponents $d - d_s$ and μ for the two quantities are in agreement. However, assuming large corrections to scaling, the data can also be fitted to the RSB picture.

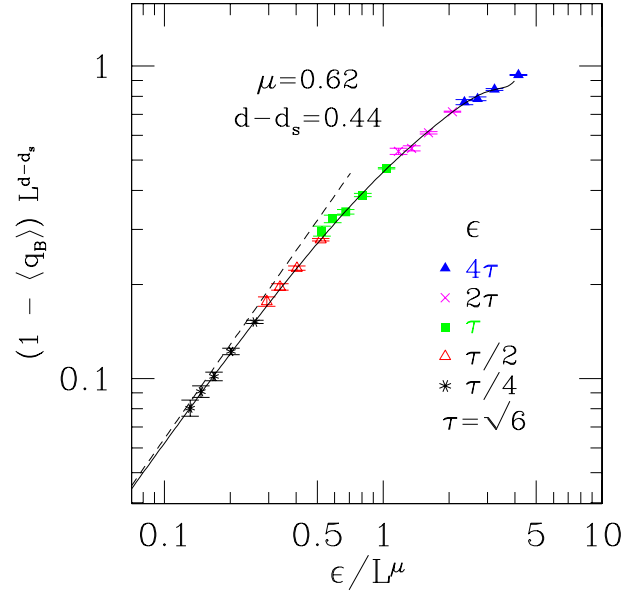


FIG. 8: Scaling plot of the box-overlap according to Eq. (32). The continuous line is a polynomial fit of order $n = 6$, which gives $\chi^2/\text{d.o.f} = 0.63$, and a goodness-of-fit parameter $Q = 0.85$. The dashed line is the linear term of the polynomial fit, corresponding to the asymptotic behavior for $L \rightarrow \infty$.

C. Comparison with periodic boundary conditions

In order to assess the effect of different boundary conditions, we have repeated part of the analysis above for the data of PY (Ref.8) for periodic boundary conditions and $L \leq 8$. The ground states were obtained using a hybrid genetic algorithm as described in PY. This does not guarantee to find the true ground state, but the systematic errors due to occasionally missing it are smaller than the statistical errors⁸.

Figs. 9 and 10 show the equivalent of Figs. 4 and 5 for periodic bc. The data in Fig. 9 shows much less curvature and also a smaller dependence on ϵ than the corresponding data for free bc in Fig. 4, indicating that corrections to scaling and deviations from the asymptotic scaling are smaller for periodic bc. Table III reports the best fits using the three functional forms of Eq. (23). Form I fits well the data, but a varies significantly with ϵ , and for small ϵ it is compatible with zero. Form II also fits well, with a independent of ϵ within the statistical errors. From this fit we estimate

$$\lim_{L \rightarrow \infty} \langle 1 - q_l \rangle_c = 0.28 \pm 0.03 \quad (\text{RSB}) \quad (39)$$

which agrees with the estimate 0.24 of Marinari and Parisi⁹, and is just consistent with our estimate 0.20 ± 0.02 for free bc.

The power law fit with no corrections, Form III, fits well the data for the two smallest values of ϵ and, if we

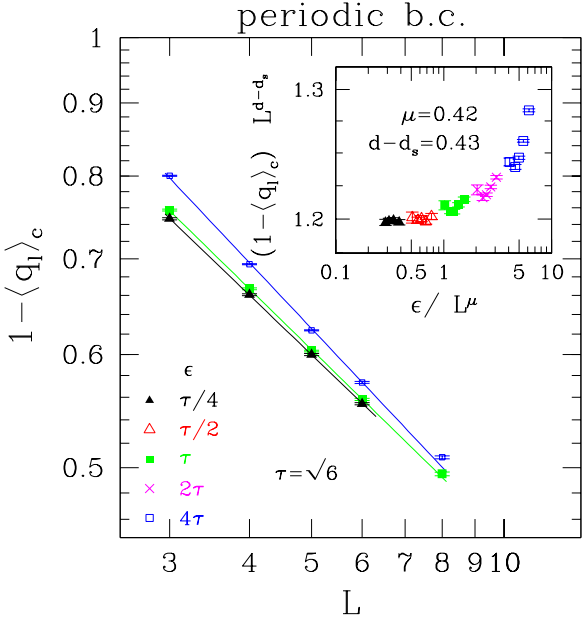


FIG. 9: Same as Fig. 4 but for periodic boundary conditions, using the data of PY (Ref.8).

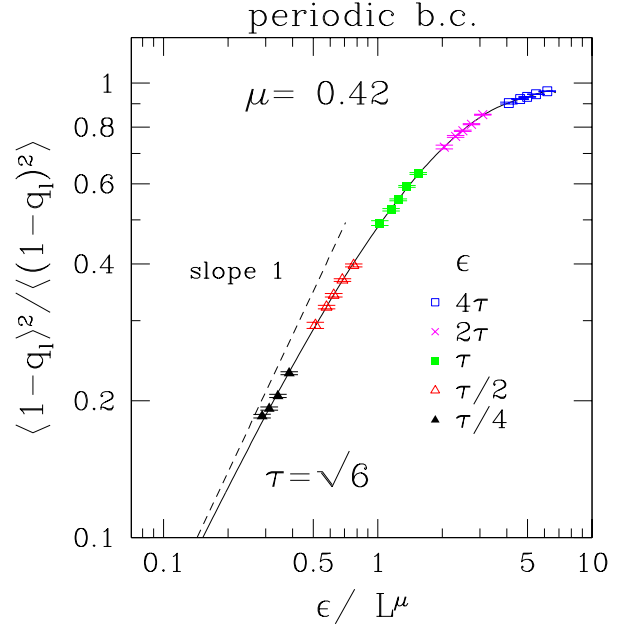


FIG. 10: Same as Fig. 5 but for periodic boundary conditions, using the data of PY (Ref.8).

exclude $L = 3$, for all but the largest value of ϵ . The exponent $c \equiv d - d_s$ is nearly independent of ϵ and gives

$$d - d_s = 0.43 \pm 0.02 \quad (\text{periodic bc}). \quad (40)$$

This result is in agreement with the estimate $d - d_s = 0.42 \pm 0.02$ of PY obtained from the ratio R defined above, confirming that corrections due to small droplets should not be important in three dimensions, and with our estimate $d - d_s = 0.44 \pm 0.03$ for free bc, indicating that $d - d_s$ does not depend on boundary conditions.

We also performed fits with Form IV which includes corrections to scaling. The results for $d - d_s = 0.43$ are shown in Table III. For the two smaller values of ϵ , the fits are difficult because corrections to scaling are very small.

We determined the exponent μ from the ratio B using Eq. (28) and the fitting procedure described for free bc, obtaining

$$\mu = 0.42 \pm 0.03 \quad (\text{periodic bc}) \quad (41)$$

in agreement with the estimate $\mu = 0.44 \pm 0.02$ of PY obtained from the scaling of the spin-overlap but incompatible, within the statistical error bars, with the result $\mu = 0.63 \pm 0.03$ for free bc. Scaling is rather satisfactory as shown in Fig. 10 (see below). The inset of Fig. 9 shows that, with these values of μ and $d - d_s$, the scaling form for $\langle 1 - q_l \rangle_c$, Eq. (14), is also well satisfied. Finally, we verified that, if $d - d_s = 0.43$, the unrestricted average $\langle 1 - q_l \rangle$ satisfies scaling, giving $\mu = 0.45 \pm 0.02$ in agreement with the estimate from B .

Form	ϵ/τ	χ^2	Q	a	b	c
I	0.25	0.003	0.99	-0.076(7)	1.256(6)	0.384(4)
	0.5	0.92	0.62	0.05(4)	1.16(2)	0.47(3)
	1	1.58	0.45	0.10(3)	1.16(2)	0.52(3)
	2	2.20	0.33	0.12(3)	1.18(2)	0.54(4)
	4	1.58	0.45	0.20(2)	1.270(4)	0.68(2)
II	0.25	0.33	0.56	0.279(7)	1.90(5)	-1.5(1)
	0.5	5.22	0.073	0.28(1)	1.90(9)	-1.5(2)
	1	0.69	0.71	0.280(4)	1.89(3)	-1.40(6)
	2	0.04	0.98	0.283(1)	1.90(1)	-1.33(2)
	4	0.36	0.83	0.291(2)	1.86(2)	-1.01(4)
III	0.25	0.02	0.887		1.204(2)	0.433(1)
	0.5	0.35	0.838		1.193(3)	0.427(2)
	1	5.14	0.076		1.21(2)	0.434(6)
	2	7.82	0.020		1.24(2)	0.440(8)
	4	25.7	$2 \cdot 10^{-6}$		1.31(2)	0.46(1)
IV	1	3.59	0.16	1.205(4)	0.3(1.5)	3(4)
	2	4.69	0.09	1.214(7)	0.2(5)	2(2)
	4	8.38	0.01	1.231(8)	0.7(5)	2.3(7)

TABLE III: Fits to $\langle 1 - q_l \rangle_c$ with $q_{\min} = 0$ and $q_{\max} = 0.4$ for periodic boundary conditions. The three groups of data refer, from top to bottom, to the three fitting functions I, II, and III in Eq. (23), respectively, and Form IV in Eq. (25) with $d - d_s = 0.43$.

Combining Eqs. (40) and (41), we obtain the estimate of θ' for periodic bc:

$$\theta' = \mu - (d - d_s) = -0.01 \pm 0.03 \quad (\text{periodic bc}). \quad (42)$$

This is compatible with zero and, within the error bars, incompatible with the value $\theta' = \theta \simeq 0.2$ characterizing the energy of domain walls induced by boundary condition changes. A scenario in which $\theta' = 0$ and $d - d_s > 0$ is consistent with the TNT picture. Although our analysis of the data in PY uses different quantities to extract exponents, our results are the same as those given by PY.

By contrast, our estimate for free bc is $\theta' = 0.19 \pm 0.06$, consistent with the droplet picture. Since θ' should not depend on the type of boundary conditions, the discrepancy must be due to different finite-size corrections using different boundary conditions. On the other hand, note the puzzling fact that the scaling plots of B for free bc (Fig. 5) and periodic bc (Fig. 10) are both quite good, but the values of μ are incompatible. Of course, if RSB is the correct hypothesis, the observed scaling would be accidental since in RSB $\mu = 0$ and the L dependence is entirely due to corrections to scaling.

In the rest of this section we try to assess the magnitude of the corrections to scaling for the different boundary conditions. In Fig. 11 we plot together the $\langle 1 - q_l \rangle_c$ data of Fig. 4 and 9 for free and periodic bc. The data for free bc lie significantly below those for periodic bc, indicating that the surface of the excitations is smaller for free bc. For periodic bc, the domain wall has to “bend” to return to the same point on the “top surface” as it had on the “bottom surface”. This may be the source of the extra surface area.

In general, it is reasonable to expect that there are some corrections to scaling which are larger for free bc, because these bc have a free surface on which lie a fraction of sites which is quite substantial for moderate sizes. For the same reason, the asymptotic behavior would set in for larger L . The latter supposition is consistent with Fig. 11 where the data for free bc clearly deviate more strongly from the asymptotic ϵ -independent behavior than the data for periodic bc. Evidence that free bc have larger corrections was also found recently in Monte Carlo simulations²⁹.

Under the hypothesis $d - d_s \simeq 0.44$, then the data of Fig. 11 are consistent with the natural hypothesis that free bc have larger corrections (since they have a larger curvature). On the other hand, if RSB is the correct asymptotic picture *and* the $L \rightarrow \infty$ limit of $\langle 1 - q_l \rangle_c$ is the same for periodic and free bc, then Fig. 11 would indicate that the corrections are *smaller* for free bc (since the data are closer to their non-zero asymptotic value) which is not very plausible. Note, however, that we do not have an argument why in the thermodynamic limit $\langle 1 - q_l \rangle_c$ should be independent of boundary conditions.

Due to the evidence that free bc have larger corrections, it is conceivable that the positive value of θ' obtained in this case is also an effect of finite size correc-

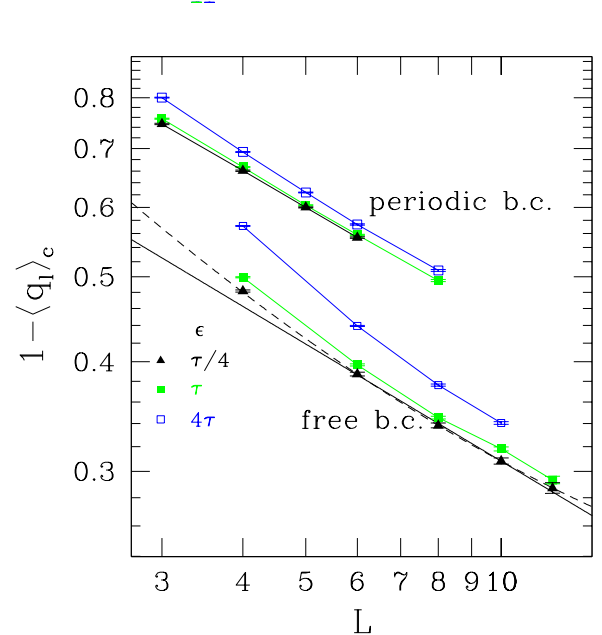


FIG. 11: This plot shows together the data of Fig. 4 for free boundary conditions and Fig. 9 for periodic boundary conditions.

tions, and hence we cannot rule out a crossover to the TNT picture for larger sizes.

This concludes the first part of this paper, dedicated to the physical results. In the next two sections, we will describe the branch and cut algorithm employed, and analyze its performance in our computations.

IV. BRANCH AND CUT ALGORITHM

Branch and cut is, to our knowledge, the fastest exact method for determining ground states of spin glasses in three dimensions. To apply this technique, we transform the problem of minimizing the Hamiltonian in Eq.(1) into a standard combinatorial optimization problem known as the *maximum cut* problem. (For a detailed description of optimization and related topics, see Ref. 30.) Consider the interaction graph $G = (V, E)$ associated with the spin glass Hamiltonian, where G contains vertices $1, \dots, L^3 \in V$ associated with the spin sites and edges $(ij) \in E$ with weight $c_{ij} = -J_{ij}$ associated with the couplings.

Given a partition of V into two sets, $W \subset V$ and its complement $V \setminus W$, the *cut* $\delta(W)$ associated with W is defined as the set of edges with one endpoint, i say, in W and the other endpoint, j say, in $V \setminus W$. In formulas, $\delta(W) = \{(ij) \in E \mid i \in W, j \in V \setminus W\}$. The *weight* of a cut $\delta(W)$ is defined as the sum of the weights of the cut edges $\sum_{(ij) \in \delta(W)} c_{ij}$. A *maximum cut* is a cut with maximum weight among all partitions W . It is easy to show that minimizing the Hamiltonian Eq.(1) is equiva-

lent to finding a maximum cut in G , see Ref. 19. If we know a maximum cut with node partition W and $V \setminus W$, the corresponding ground state spin configuration can be read off by assigning the value up to the spins in W and down to the spins in $V \setminus W$, or vice versa.

The branch-and-cut algorithm solves the maximum cut problem through simultaneous lower and upper bound computations. By definition, the weight of any cut gives a *lower bound* on the optimal cut value. Thus, we can start from any cut and iteratively improve the lower bound using deterministic heuristic rules (local search and other specialized heuristics, see Ref. 31 for details). How do we decide when a cut is optimal? This can be done by additionally maintaining *upper bounds* on the value of the maximum cut. Upon iteration of the algorithm, progressively tighter bounds are found, until optimality is reached.

Since the availability of upper bounds marks the difference between a heuristic and an exact solution, we now summarize how the upper bound is computed (for more details, see Ref. 31.) To each edge (ij) we associate a real variable x_{ij} and to each cut $\delta(W)$ an *incidence vector* $\chi^{\delta(W)} \in \mathbb{R}^E$ with components $\chi_{ij}^{\delta(W)}$ associated to each edge (ij) , where $\chi_{ij}^{\delta(W)} = 1$ if $(ij) \in \delta(W)$ and $\chi_{ij}^{\delta(W)} = 0$ otherwise. Denoting by $P_C(G)$ the convex hull of the incidence vectors, it can be shown that a basic optimum solution³² of the linear program

$$\max \left\{ \sum_{(ij) \in E} J_{ij} x_{ij} \mid x \in P_C(G) \right\}. \quad (43)$$

is a maximum cut. In order to solve (43) with linear programming techniques we would have to express $P_C(G)$ in the form

$$P_C(G) = \{x \in \mathbb{R}^E \mid Ax \leq b, 0 \leq x \leq 1\} \quad (44)$$

for some matrix A and some vector b . Whereas the existence of A and b are theoretically guaranteed, even subsets of $Ax \leq b$ known in the literature contain a huge number of inequalities that render a direct solution of (43) impractical.

Instead, the branch-and-cut algorithm proceeds by optimizing over a *superset* P containing $P_C(G)$, and by iteratively tightening P , generating in this way progressively better upper bounds. The supersets P are generated by a *cutting plane* approach. Starting with some P , we solve the linear program $\max \left\{ \sum_{(ij) \in E} J_{ij} x_{ij} \mid x \in P \right\}$ by Dantzig's simplex algorithm³². Optimality is proven if either of two conditions is satisfied: (i) the optimal value equals the lower bound; (ii) the solution vector \bar{x} is the incidence vector of a cut.

If neither is satisfied, we have to tighten P by solving the *separation problem*. This consists in identifying inequalities that are valid for all points in $P_C(G)$, yet are violated by \bar{x} , or reporting that no such inequality exists. The inequalities found in this way are added to the linear programming formulation, obtaining a new tighter

partial system $P' \subset P$ which does not contain \bar{x} . The procedure is then repeated on P' and so on.

At some point, it may happen that (i) and (ii) are not satisfied, yet the separation routines do not find any new cutting plane. In this case, we *branch* on some fractional edge variable x_{ij} (i.e. a variable $x_{ij} \notin \{0, 1\}$), creating two subproblems in which x_{ij} is set to 0 and 1, respectively. We then apply the cutting plane algorithm recursively for both subproblems.

V. PERFORMANCE OF THE BRANCH AND CUT ALGORITHM

In this section we study the performance of our current implementation of the branch and cut algorithm, in particular the dependence of the number of computer operations on system size. However, the results for size $L = 12$ were obtained with a more efficient version of the code, so performance for this size cannot be compared with that for the smaller sizes. Hence, in this section, we shall just consider sizes up to $L = 10$.

Finding the ground state of the Hamiltonian Eq. (1) in three dimensions is an \mathcal{NP} -hard problem²¹, and all known algorithms to solve this class of problems require a number of operations that grows exponentially on the size of the input, in the worst case.

However, depending on the problem, the number of operations for *typical* instances (for the spin glass problem, an instance is a realization of the random couplings, or sample), can grow considerably more slowly than the worst case exponential behavior. Furthermore, the number of operations can vary significantly from one instance to another. It is therefore useful to investigate experimentally the performance of the algorithm for typical instances, in order to try to extrapolate the computational resources necessary to go to larger sizes, and possibly to identify which parameters of the problem affect most the performance. De Simone et al.¹⁹ measured the average CPU time used by the branch and cut algorithm to find the ground state of the two-dimensional $\pm J$ spin glass with periodic bc, up to $L = 70$, showing that the average CPU time was approximated by a function proportional to L^6 .

Here we analyze the performance of the branch and cut algorithm for the three-dimensional spin glass with free bc and Gaussian couplings. In order to do this, we first need a good measure of the performance. For a complex algorithm such as branch and cut, a simple and absolute measure of the number of operations is not available. Two possible measures are the CPU time and the number of linear programs solved during the run of the algorithm. In Table IV, we summarize the average running time needed for calculating an unperturbed ground state for the different system sizes.

The CPU time is not an accurate measure since it depends on the machine architecture and load. Furthermore, our computations were carried out on several dif-

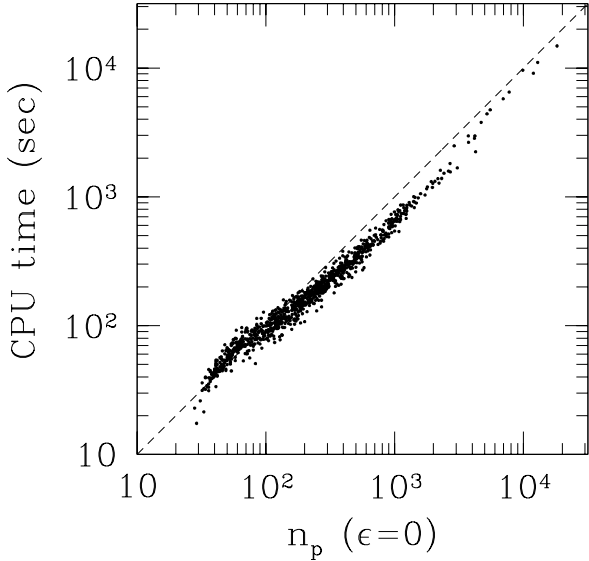


FIG. 12: Scatter plot of the CPU time to find the unperturbed ground state ($\epsilon = 0$) versus the corresponding number of linear programs solved (n_p). Each point represents a randomly generated sample with $L = 10$. All the computations for this set of samples were run on the same machine. The dashed line indicates a linear behavior.

L	mean CPU time per sample
4	0.065
6	0.662
8	10.11
10	338

TABLE IV: Mean CPU time per sample in seconds for the calculation of the unperturbed ground state, averaged also over the different machines.

ferent machines, so the CPU time is not useful here. We take instead the number of linear programs solved, n_p , because (i) it is a well-defined and machine independent quantity; (ii) we have observed that about 95% of the time is spent in solving linear programs; (iii) for a fixed system size, n_p correlates strongly, and almost linearly, with the CPU time. This is shown in Fig. 12, which plots the CPU time versus n_p for 1000 randomly generated samples with $L = 10$, computed on the same machine. Note that since the size of the linear programs is also growing with the system size, the CPU time per linear program increases strongly with L , as shown in Table V. Hence, n_p severely underestimate the rate at which the number of operations increases with L .

From Fig. 12, we also note that the distribution of n_p (and CPU times) is very broad, extending over three

L	mean CPU time per lp	median CPU time per lp
4	0.00770	0.0044
10	0.833	0.784

TABLE V: Mean and median CPU time in seconds per linear program for finding the unperturbed ground state for samples computed on the same machine.

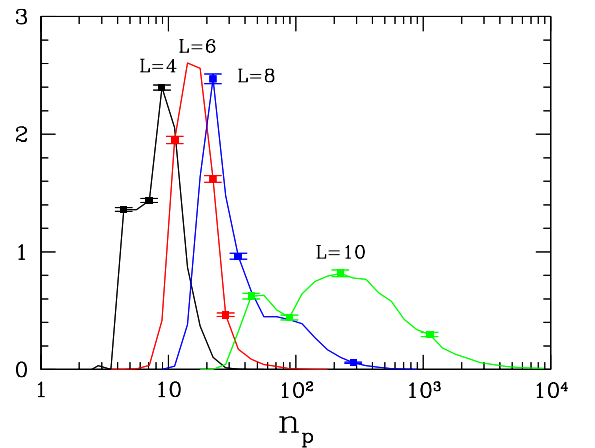


FIG. 13: Histogram of the number of linear programs solved by the branch and cut algorithm to find the unperturbed ground state for different system sizes.

orders of magnitude. The histogram distribution of n_p for different system sizes is shown in Fig. 13. In addition to shifting to larger n_p , the distribution broadens as L increases. Also, there is some evidence of a double-peak structure. For $L = 10$, we verified that the peak at smaller n_p corresponds to samples that could be solved without branching, while the other peak corresponds to samples where branching was necessary. Since in each branching step the number of subproblems to be solved doubles, the number of linear programs increases rapidly and the second peak is at significantly larger n_p .

In order to identify which parameters of the problem, in addition to the size, affect the performance, we ask whether n_p correlates with the physical observables we measure. No significant correlation was observed with the ground state energy. Fig. 14 plots³³ $\langle \log_{10} n_p \rangle$ for the unperturbed ground state ($\epsilon = 0$) and $L = 10$ versus the overlap between this state and the perturbed ground state with $\epsilon/\tau = 4$. We observe a distinct correlation between n_p and q : for small q , more linear programs are needed than for large q . The figure shows that the

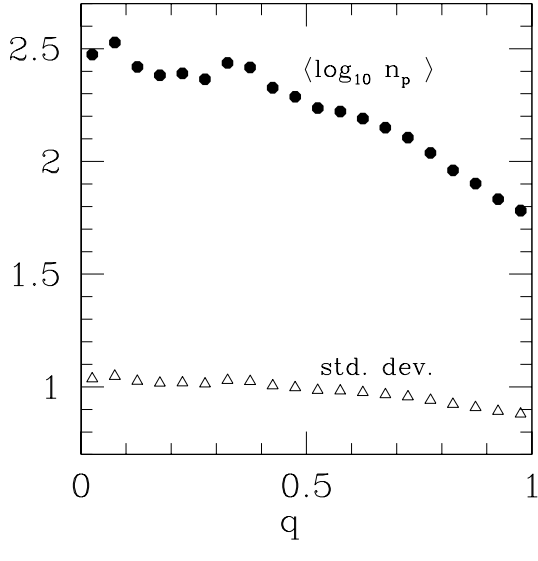


FIG. 14: The circles are a plot of $\langle \log_{10} n_p \rangle$, where n_p is the number of linear programs solved to compute the unperturbed ground state S^0 , versus the overlap between $S^{(0)}$ and the perturbed ground state $\tilde{S}^{(0)}$. The data is for $\epsilon/\tau = 4$ and the samples were selected from a set of randomly generated samples with $L = 10$, in such a way that the same number of samples is plotted for each consecutive q interval of length 0.1, in order to sample equally all regions of q . The triangles show the standard deviation, among samples, of $\log_{10} n_p$ as a function of q .

typical number of linear programs is close to an order of magnitude larger if $q \simeq 0$ than if $q \simeq 1$. We observed a similar correlation for other values of ϵ as well, and also between the CPU time and q . Again, the distribution of n_p is quite broad as shown by the data for the standard deviation of $\log_{10} n_p$ in Fig. 14.

In order to quantify how the correlation between n_p and q changes with the system size, we show in Fig. 15 the average and median of n_p as a function of N_b , as well as the conditional averages of n_p restricted to samples with large ($|q| \geq 0.9$) and small ($|q| \leq 0.1$) overlap. We take the number of bonds, N_b , as a measure of the input size, since the maximum cut problem is specified in terms of the edge variables in the graph. First, all measures show an approximately exponential increase with N_b , with corrections for small N_b . Second, the difference between the conditional averages with small and large q seems to increase with the system size, and is about one order of magnitude for $L = 10$.

A qualitative difference between samples with small and large overlap is that samples with a small $|q|$ have a rougher “energy landscape”, namely states with an energy close to the ground state energy yet a spin configuration very different from the ground state. It is then intu-

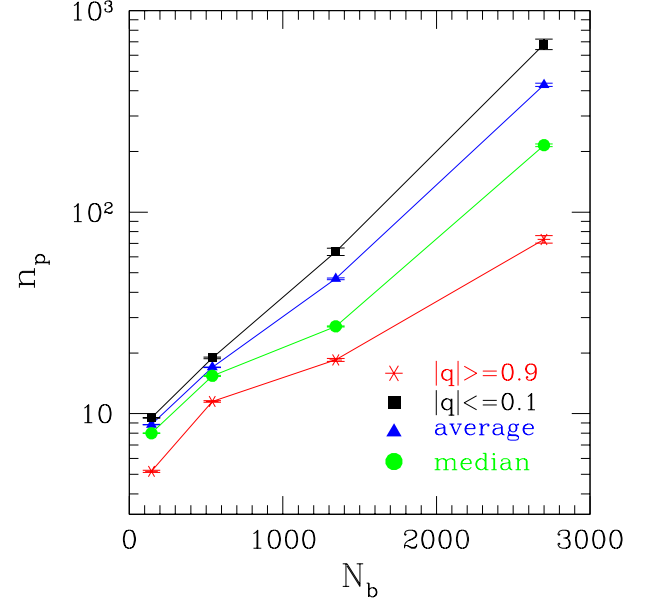


FIG. 15: Average n_p , median n_p , and conditional averages of n_p restricted to $|q| \leq 0.1$ and to $|q| \geq 0.9$, as a function of N_b . The data for n_p are for $L = 10$ and $\epsilon = 0$ (unperturbed ground state), and q is the overlap between the $\epsilon = 0$ and $\epsilon/\tau = 4$ ground states.

itively clear why one would observe a correlation between q and the running time for a stochastic algorithm employing local search heuristics, such as simulated annealing, since when the algorithm encounters one of these configurations with small overlap, it must retrace its steps by a large amount.

However, for the branch and cut algorithm, a reason for the correlation between n_p and q is less obvious, but some insight is provided by an analysis of “reduced cost fixing”. This is a feature of the branch and cut algorithm speeding up the computations. In every iteration of the algorithm, reduced cost fixing gives us a sufficient condition to decide which variables (corresponding to the edges in the graph) have already attained their optimal value. Therefore, we can fix the variables with “optimal” status to their current value for all the subsequent iterations of the algorithm, resulting in less overall computational effort. The more variables that can be fixed, the faster the algorithm is in practice.

Since the samples with small overlap have “almost optimal” solutions with spin configurations very different from the ground state, a smaller number of variables can be fixed. Here we do not have the “correct” edge values available until the end. As an example, we checked that for $L = 10$ and $\epsilon = \tau$, for 100 randomly chosen samples with small overlap ($|q| \leq 0.1$), in average 409 ± 39 of the 2700 edge variables could be fixed in the first sub problem, i.e. before branching takes place. In contrast, for 100 randomly chosen samples with big overlap ($|q| \geq 0.9$),

921 ± 34 of the edge variables could be fixed in the first sub problem, about twice as many. Of course, the less variables that can be fixed in the first sub problem, the more overall branching is necessary, resulting in more overall computational effort for samples with small overlap.

A consequence of the broad distribution of the CPU time and of its correlation with the physical observables of interest, is that a cutoff in the CPU time produces a systematic error in these quantities. One has therefore to ensure that the cutoff is large enough so that the systematic error is smaller than the statistical error.

It is interesting to try to extrapolate the running time needed to deal with larger sizes. The average CPU time in Table IV varies approximately as $\sim \exp(\alpha N_b)$ with α somewhere between 0.0024 and 0.003. Extrapolating to $L = 14$ ($N_b = 7644$), this gives an average CPU time of around $10^{8 \pm 1}$ seconds per sample, which is clearly very demanding. Furthermore, memory limitations will set in before we can reach this size. Again, note that n_p increases much more slowly with N_b . The data for $|q| \leq 0.1$ in Fig.15, for example, vary approximately as $\sim \exp(\alpha N_b)$ with a smaller α around 0.0017, showing that the dominant limiting factor is the solution of the linear programs. Note that the program used for $L = 12$ is significantly faster than that used in this extrapolation. This long extrapolated running time gives us further motivation to continue our research on the improvement of this algorithm.

VI. CONCLUSIONS

Using an *exact* “branch and cut” optimization algorithm, we have studied the large-scale, low-energy excitations in the Ising spin glass in three dimensions with *free* boundary conditions, and compared the results with those obtained earlier by PY for periodic boundary conditions.

For both types of boundary conditions, the data are well described by a general scaling picture involving only two scaling exponents, $d - d_s$ and θ' , with only small corrections to scaling. Some observables show significant corrections to *asymptotic* scaling, which are larger for free

boundary conditions. Fitting this scaling picture to our data, we obtain comparable values of $d - d_s$ for periodic (0.43 ± 0.02) and free boundary conditions (0.44 ± 0.03).

However, for periodic boundary conditions we obtain $\theta' \simeq 0$, which fits well the TNT scenario ($d - d_s > 0, \theta' = 0$), while for free boundary conditions we obtain $\theta' = 0.19 \pm 0.06$, which fits well the droplet picture ($d - d_s > 0, \theta' > 0$). Data for the box overlap for free boundary conditions indicates smaller corrections to asymptotic scaling, which is reasonable since the box is away from the surface, but the data still favors the droplet picture if one assumes that corrections to scaling are indeed small.

Since it is unlikely that the correct physical scenario depends on boundary conditions, this indicates that one of the boundary conditions, probably free, has large undetected corrections to scaling. Therefore our data for free boundary conditions do not rule out the TNT picture.

For both free and periodic bc, the data are also fitted well by the RSB picture ($d - d_s = 0, \theta' = 0$), but only if we allow very large corrections to scaling. In this case, the good scaling behavior we observed would only be a finite size artifact, and would disappear at larger sizes. To test this possibility, large system sizes will be needed.

Finally, we have analyzed the performance of the branch and cut algorithm, finding that the performance is worse when there is a low energy excited state close in energy to the ground state but far away in configuration space, and have given a quantitative analysis of this effect.

Acknowledgments

We would like to thank A. J. Bray, G. Parisi, M. Mézard, D. S. Fisher, and M. A. Moore for helpful discussions and correspondence. APY acknowledges support from the NSF through grant DMR 0086287. MP would like to thank A. J. Bray for a useful suggestion on the data analysis. We thank the Regional Centre of Computing of the University of Cologne for the allocation of computer time. Over the years, Giovanni Rinaldi and Gerd Reinelt contributed much to the algorithm.

¹ D. S. Fisher and D. A. Huse, J. Phys. A. **20** L997 (1987); D. A. Huse and D. S. Fisher, J. Phys. A. **20** L1005 (1987); D. S. Fisher and D. A. Huse, Phys. Rev. B **38** 386 (1988).

² A. J. Bray and M. A. Moore, in *Heidelberg Colloquium on Glassy Dynamics and Optimization*, L. Van Hemmen and I. Morgenstern eds. (Springer-Verlag, Heidelberg, 1986).

³ W. L. McMillan, J. Phys. C, **17**, 3179 (1984).

⁴ G. Parisi, Phys. Rev. Lett. **43**, 1754 (1979); J. Phys. A **13**, 1101, 1887, L115 (1980); Phys. Rev. Lett. **50**, 1946 (1983).

⁵ M. Mézard, G. Parisi and M. A. Virasoro, *Spin Glass Theory and Beyond* (World Scientific, Singapore, 1987).

⁶ K. Binder and A. P. Young, Rev. Mod. Phys. **58** 801

(1986).

⁷ F. Krzakala and O. C. Martin, Phys. Rev. Lett. **85**, 3013 (2000), (referred to as KM).

⁸ M. Palassini and A. P. Young, Phys. Rev. Lett. **85**, 3017 (2000), (referred to as PY).

⁹ E. Marinari and G. Parisi, Phys. Rev. Lett. **86**, 3887 (2001).

¹⁰ A. A. Middleton, Phys. Rev. B **63**, 060202(R) (2001).

¹¹ H. G. Katzgraber, M. Palassini and A. P. Young, Phys. Rev. B **63**, 184422, (2001).

¹² C. M. Newman and D. L. Stein, Phys. Rev. B **46**, 973 (1992); Phys. Rev. Lett., **76** 515 (1996); Phys. Rev. E **57**

1356 (1998).

¹³ C.M. Newman and D.L. Stein, Phys. Rev. Lett. **87**, 077201-1, (2001)

¹⁴ J. Lamarcq, J.-P. Bouchaud, O. C. Martin and M. Mezard, Europhys. Lett. 58(3), 321 (2002).

¹⁵ M. A. Moore, cond-mat/0203469.

¹⁶ M. Jünger, G. Reinelt and S. Thienel, in *DIMACS Series in Discrete Mathematics and Theoretical Computer Science*, Volume 20, W. Cook, L. Lovasz and P. Seymour eds. (American Mathematical Society, 1995)

¹⁷ S. Kobe and A. Hartwig, Comp. Phys. Comm. **16**, 1 (1978).

¹⁸ M. Alava, P. Duxbury, C. Moukarzel, H. Rieger, Combinatorial optimization and disordered system, in *Phase Transition and Critical Phenomena*, Vol. 18, p. 141-317, ed. C. Domb and J.L. Lebowitz, Academic Press, Cambridge (2000).

¹⁹ C. De Simone, M. Diehl, M. Jünger, P. Mutzel, G. Reinelt and G. Rinaldi, J. Stat. Phys. **80**, 487 (1995)

²⁰ F. Liers and M. Jünger, Int. J. Phys. C **11**, 589 (2000).

²¹ F. Barahona, J. Phys. A. **15** 3241 (1982).

²² In reality, our implementation of the branch and cut algorithm works as follows: If we have found the optimal configuration, i.e. two sets of spins where all spins in one set point up and all spins in the other point down, we assign the value “up” to the set with the smaller cardinality. Therefore we do not produce a symmetrical distribution. This does not affect the analysis since we are interested only in the absolute value of the overlap.

²³ M. Palassini, 2000, unpublished.

²⁴ This average does not coincide with the midpoint of the interval because the perturbation method does not sample uniformly in q .

²⁵ These errors do not take into account correlations between the different fit parameters, and hence underestimate considerably the the actual statistical uncertainty of the fit parameters.

²⁶ A. K. Hartmann, Phys. Rev. E **59**, 84 (1999). A. J. Bray and M. A. Moore, J. Phys. C, **17**, L463 (1984); W. L. McMillan, Phys. Rev. B **30**, 476 (1984).

²⁷ E. Marinari, G. Parisi, F. Ricci-Tersenghi, J.J. Ruiz-Lorenzo, J. Phys. A **31**, L481 (1998).

²⁸ M. Palassini and A.P. Young, unpublished.

²⁹ H.G. Katzgraber and A.P. Young, Phys. Rev. B **65**, 214402, (2002).

³⁰ M. Jünger and D. Naddef, eds., *Computational Combinatorial Optimization* (Lecture Notes in Computer Science 2241, Tutorial, Springer Verlag Heidelberg, 2001).

³¹ F. Barahona, M. Grötschel, M. Jünger, G. Reinelt, Operations Research, **36** 493-513 (1988).

³² V. Chvátal, *Linear Programming* (Freeman, New York) 1983.

³³ The perturbation method does not generate a uniform distribution of q , therefore Fig. 14 was produced by selecting 1000 samples from a random ensemble, such that there is the same number of samples in each consecutive q interval of length 0.1 in the range $q \in [-1, 1]$.